Locally Distributed Digital Real-Time Power System Co-simulation via Multi-phase Distributed Transmission Line Model

Locally Distributed Digital Real-Time Power System Co-simulation via Multi-phase Distributed Transmission Line Model

Luca Barbierato, Steffen-Vogel, Daniele Salvatore Schiera, Enrico Pons, Lorenzo Bottaccioli, Antonello Monti, and Edoardo Patti

***Abstract*—The intrinsic complexity of smart grids requires computer-aided power system analysis to evaluate novel monitoring and control strategies and innovative devices. Due to the enormous computational requirements and the necessary Hardware-In-the-Loop (HIL) and Power Hardware-In-the-Loop (PHIL) applications, real-time power system simulation plays a fundamental role in this context. However, performing real-time simulations in a monolithic way, i.e. exploiting a single Digital Real-Time Simulator (DRTS) rack, could result in the inability to create reliable and accurate digital twins of increasingly complex power systems such as smart grids. This paper proposes a locally distributed digital real-time power system co-simulation to link different DRTS and scale up the viable Power System Under Test (PSUT). It exploits Aurora 8B/10B to manage the data exchange and a Distributed Transmission Line Model (DTLM) to split the PSUT into the two real-time simulation environments. Furthermore, the multi-phase DTLM permits the absorption of the communication latency, which normally occurs in real-time co-simulation, into the propagation model of a transmission line. With the presented setup, a time step duration of $50\,\mu s$ proves to be stable and accurate when running a co-simulated Electro-Magnetic Transients (EMT) analysis of a power grid scenario by interconnecting two commercial DRTS (i.e. OPAL-RT) with comparable results compared to the monolithic simulation, extending the scalability of future real-time smart grid simulations.**

***Index Terms*—Power System, Digital Real-Time Simulator, Co-simulation Techniques, Distributed Transmission Line Model**

ACRONYMS

CPU	Central Processing Unit
DRTS	Digital Real-Time Simulator
DTLM	Distributed Transmission Line Model
DER	Distributed Energy Resources
DIM	Dumping Impedance Method
EMTP	Electro-Magnetic Transients Program
EMT	Electro-Magnetic Transients
E2E	End-to-End
GPS	Global Positioning System
HIL	Hardware-In-the-Loop
ITM	Ideal Transformer Method
IA	Interface Algorithm
LAN	Local Area Network
MAPE	Mean Absolute Percentage Error
PSUT	Power System Under Test
PHIL	Power Hardware-In-the-Loop
PTP	Precision Time Protocol
RLC	resistive, inductive, and capacitive
SFP	Small-form Factor Pluggable
TC	Transparent Clock

L. Barbierato and E. Patti are with the *Department of Control and Computer Engineering*, Politecnico di Torino, Turin, Italy (e-mail: name.surname@polito.it).

S. Vogel and A. Monti are with the E.ON Energy Research Center, RWTH Aachen University, Aachen, Germany (svogel2@eonerc.rwth-aachen.de).

D. S. Schiera and E. Pons are with the *Department of Energy*, Politecnico di Torino, Turin, Italy (e-mail: name.surname@polito.it).

L. Bottaccioli is with the *Interuniversity Department of Regional and Urban Studies and Planning*, Politecnico di Torino, Turin, Italy (e-mail: name.surname@polito.it).

L. Barbierato, D. S. Schiera, E. Pons, L. Bottaccioli, and E. Patti are with the Energy Center LAB, Politecnico di Torino, Turin, Italy (e-mail: name.surname@polito.it).

This work was partially supported by the EU H2020 Project *European Research Infrastructure supporting Smart Grid and Smart Energy Systems Research, Technology Development, Validation and Roll Out - Second Edition (EriGRID2.0)*, Grant Agreement N^o 654113.

I. INTRODUCTION

The analysis of power systems requires real-time simulation over Digital Real-Time Simulator (DRTS) for a reliable and accurate study of the complex behaviour of transmission and distribution networks. This is even further essential in the context of high penetration of Distributed Energy Resources (DER) and storages that require improving the energy systems integration [1]. DRTS technologies not only permit solving power system networks using nodal analysis but also accelerate the study and development of power system equipment through the application of HIL and PHIL. To this extent, various DRTS commercial solutions (e.g. OPAL-RT and RTDS Technologies) have been proposed to accelerate the required computation for high-intensive tasks, such as EMT analysis [2]. However, the real-time simulation of innovative smart grids requires massive computing capabilities, especially to coordinate complex systems for large-scale scenarios.

Several works in the literature have already implemented parallel computing strategies to solve EMT analysis of scalable PSUT. For instance, the MATLAB Simulink Simscape library [3] enables the partitioning of a power system by using the propagation delay of a transmission line to absorb the inherent delay required to avoid direct feedthrough. Traditional power systems present many transmission lines long enough to decouple points in the network, allowing parallel computation on multiple cores of a Central Processing Unit (CPU) [4]. The same concept is applied in ARTEMiS library [5] to split a

power system across different cores of OPAL-RT Technologies DRTS to improve their real-time scalability [6]. However, the computational capability of a single DRTS rack is limited and cannot overcome the problem of analyzing large and increasingly complex smart grid scenarios.

Therefore, the scientific community proposed to interconnect different DRTS racks through communication protocols (e.g. Ethernet) to combine their computational capabilities in a unique distributed digital real-time power system co-simulation environment [7]. Communication latencies, synchronization, and time regulation are the main issues in these interconnections, where the time step duration reaches tens of microseconds.

DRTS provide communication with the external world using standard Internet communication protocols (e.g. UDP, TCP) over the Internet [8]. So, it may be argued that a conventional Local Area Network (LAN) can be utilized for communication between DRTS. However, the architecture of DRTS and the constraints of the communication protocols limit the sampling frequency of asynchronous blocks within the simulation environment that cannot reach the typical real-time simulation frequency, subsampling the exchanged variables and losing accuracy on their representation. For instance, OPAL-RT racks are limited to a maximum frequency of $5\,\mathrm{kHz}$ for standard Internet communication protocols. It is important to note that this value should be considered as an upper limit because managing such a large amount of data requires a high network bandwidth. Additionally, the inherent latency introduced by these communication protocols can significantly impact the real-time co-simulation [9]. This latency is a stochastic process with variable jitter, dependent on the traffic congestion of the LAN network that can have a substantial effect on the real-time co-simulation [10].

New technologies must be developed to tackle this issue by allowing DRTS racks to be connected without compromising simulation performance, particularly in terms of dynamic simulation accuracy [11]. Most of the solutions proposed in the literature are inspired by the PHIL application and its stability and accuracy intrinsic issues [12], such as Interface Algorithm (IA) proposed for PHIL real-time simulation. The most suitable IA for these interconnections is the Ideal Transformer Method (ITM) [13]. In [14], Shen et al. focus on developing power system models for distributed real-time simulations exploiting ITM and delay compensation. More complex PHIL IA could enhance the stability and accuracy of the interconnection. For instance, Aguirre et al. [15] enhance the Dumping Impedance Method (DIM) by calculating the load impedance, to include it as part of the IA to enhance its accuracy and stability. However, the effect of the latency experienced by the signal exchanged (i.e. voltages and currents) and its variability still generates a noticeable non-linear effect, affecting the accuracy of the real-time co-simulation solution.

To cope with those issues, different works in the literature implement interface signal transformation to deal with time-varying delays, packet loss, and reordering caused by a shared network for communication. Stevic et al. [16] present a co-simulation interface algorithm based on a representation of interface quantities in the form of dynamic phasors. In [17] instead, wave transformation is applied to interface quantities. Other works tackle the delay compensation to reduce the inaccuracies caused by latency. For instance, the time delay compensation method presented in [18]. In the end, none of the previous solutions permits linking with flexibility different DRTS together, maintaining the accuracy of a monolithic simulation.

This paper proposes a locally distributed digital real-time power system co-simulation implementing a Multi-phase Distributed Transmission Line Model (DTLM) as an adapter to split and extend the scalability of a PSUT concerning a monolithic digital real-time simulation. The DTLM is applicable to multi-phase transmission lines with a minimum length determined by the characteristic propagation velocity ν of a single-phase line or the characteristic propagation velocity of the slower mode in multi-phase lines. The locally distributed co-simulation setup is accomplished by interconnecting two DRTS by means of an optical fiber link between their Small-form Factor Pluggable (SFP) ports, exploiting the Aurora 8B/10B protocol. Aurora, in a nutshell, ensures the minimum communication latency among the available protocols on commercial DRTS. The proposed solution absorbs the communication latency experienced during the data exchange management of the locally distributed co-simulation setup in the propagation time of the travelling wave of the DTLM. Because the communication latency is typically a multiple of the time step duration T_S depending on the commercial DRTS setup [13], the proposed Multi-phase DTLM allows for the setting of a variable communication latency attribute based on the laboratory configuration. To solve the complex time regulation, alignment, and synchronisation schemes, the locally distributed co-simulation infrastructure integrates the IEEE 1588 Precision Time Protocol (PTP) stack [19] to ensure the overall alignment of the internal reference clock of the locally distributed DRTS. This is accomplished by a Global Positioning System (GPS) Clock that allows a global synchronization with the GPS time reference and acts as a master clock of the overall laboratory.

The locally distributed digital real-time power system co-simulation has been tested over a laboratory setup with two identical commercial DRTS, called OPAL-RT OP5700, by employing an optical fiber echo link among two of their SFP ports. The proposed solution has been tested over a simple single-phase PSUT to demonstrate the stability and accuracy of the co-simulated scenario, providing identical experimental results concerning a monolithic simulation. Moreover, the multi-phase capability of the proposed DTLM has been tested on a scenario similar to the single-phase one but declined to a three-phase power system. Also in this scenario, the experimental results demonstrate identical stability and accuracy with respect to the monolithic simulation.

As possible industrial applications, this solution can be employed for simulating scalable transmission networks, where huge power systems can be split into two subsystems that are simulated separately using two DRTS without incurring typical disturbances due to the co-simulation interconnection. So, this solution enhances the analysis of large-scale systems by harnessing the combined computational capabilities of the

two DRTS. Moreover, it has the potential to foster EMT analysis of large-scale power systems in conjunction with HIL and PHIL applications. This, in turn, can lead to the emergence of innovative industrial business scenarios enabling companies to explore and validate new concepts, technologies, and operational strategies in a virtual environment before implementing them in real-world applications. This can lead to improved efficiency, reliability, and sustainability in transmission systems and contribute to the development of advanced solutions for emerging challenges in the power system sector.

With respect to our previous work [20], the key contributions and novelties proposed in this manuscript are summarised in the following.

1) A more detailed theoretical background section has been added to describe the theoretical formulation of the Electro-Magnetic Transients Program (EMTP) multi-phase transmission line model.
2) The DTLM model has been extended to manage multi-phase transmission lines, enabling more realistic scenarios than the single-phase model presented in the previous work.
3) The locally distributed digital real-time power system co-simulation has been extended to manage the proper time alignment, synchronization, and regulation among locally distributed DRTS by integrating the IEEE 1588 PTP stack offered by a commercial GPS clock.
4) The proposed scenarios have been extended including a three-phase power system to test the multi-phase capability of the novel DTLM block.
5) The experimental results have been extended by presenting new measurements concerning the transients that affect the proposed scenarios.

The structure of the manuscript is described as follows. Section III reports the methodological framework used to complete the locally distributed digital real-time power system co-simulation and develop the DTLM adapter. In Section IV, the selected PSUT is described. Section V presents experimental results on the proposed PSUT confirming the identical solution of the locally distributed digital real-time power system co-simulation via DTLM w.r.t. a monolithic simulation. Finally, Section VI reports concluding remarks and future works.

II. Theoretical Background

This section presents the theoretical formulation of the EMTP transmission line model for the sake of self-consistency and clarity of the manuscript. Firstly, the single-phase line model formulation is introduced in Figure 1 by solving the ordinary differential equations which describe line voltage and current. The three-phase line model formulation instead applies a modal transformation to eliminate the mutual coupling among phases. The resulting modes are then treated as single-phase lines to finally obtain the solution of the three-phase line model by applying a modal anti-transformation.

A. Single-phase Line

Considering a lossless single-phase line with inductance L' and capacitance C' per-unit length, the line voltage e and current i at a point x are related by the ordinary differential equations in Equation 1a and Equation 1b.

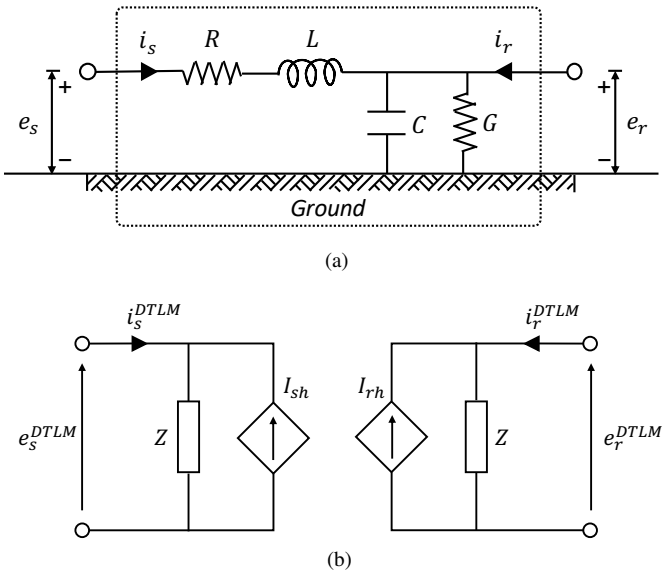

Fig. 1. Single-phase line (a) and the equivalent impedance circuit (b)

$$-\frac{\partial e(x,t)}{\partial x} = L' \frac{\partial i(x,t)}{\partial t} \tag{1a}$$

$$-\frac{\partial i(x,t)}{\partial x} = C' \frac{\partial e(x,t)}{\partial t} \tag{1b}$$

The general equations solution, first given by D'Alambert, is presented in Equation 2a and Equation 2b.

$$e(x,t) + Z_c\, i(x,t) = 2Z_c\, f_1(x - vt) \tag{2a}$$

$$e(x,t) - Z_c\, i(x,t) = -2Z_c\, f_2(x + vt) \tag{2b}$$

where $f_1(x-\nu t)$ and $f_2(x-\nu t)$ are arbitrary functions of the variable $(x-vt)$ and $(x+vt)$. For the lossless single-phase line, the wave propagation v is equal to $1/\sqrt{L'\,C'}$ and the surge impedance Z_c is equal to $\sqrt{L'/C'}$. The physical interpretation of these equations describes the voltage e and current i as a wave travelling at velocity ν in a forward direction (i.e. Equation 2a) and a wave travelling in a backward direction (i.e. Equation 2b). In [21], Equation 2a and Equation 2b are solved by exploiting the characteristic of the differential equations, that is when the forward travelling wave is observed by travelling along the line with velocity v. From this perspective, the quantity $e+Z_c\, i$ must arrive unchanged at the other subsystem after a transport delay τ, which is given by Equation 3.

$$\tau = \frac{d}{\nu} \tag{3}$$

where d is the length of the line and ν is the propagation speed. The resulting model equations for a lossless single-phase line (i.e. $R' = 0$) are:

$$e_r(t) - Z_c\, i_r(t) = e_s(t-\tau) - Z_c\, i_s(t-\tau) \tag{4a}$$

$$e_s(t) - Z_c\, i_s(t) = e_r(t-\tau) - Z_c\, i_r(t-\tau) \tag{4b}$$

knowing that:

$$i_s(t) = \frac{e_s(t)}{Z} - I_{sh}(t) \tag{5a}$$

$$i_r(t) = \frac{e_r(t)}{Z} - I_{rh}(t) \tag{5b}$$

in a lossless line, the two current sources I_{sh} and I_{rh} are computed as:

$$I_{sh}(t) = \frac{2}{Z_c}\, e_r(t-\tau) - I_{rh}(t-\tau) \tag{6a}$$

$$I_{rh}(t) = \frac{2}{Z_c}\, e_s(t-\tau) - I_{sh}(t-\tau) \tag{6b}$$

When losses are taken into account, new equations for I_{sh} and I_{rh} are obtained by lumping $R/4$ at both ends of the line and $R/2$ in the middle of the line where R is the total resistance of the line:

$$R = R'\, d \tag{7}$$

where R' is the characteristic resistance per unit length. The current sources I_{sh} and I_{rh} are then computed as follows:

$$I_{sh}(t) = \left(\frac{1+h}{2}\right)\left(\frac{1+h}{Z}\, e_s(t-\tau) - h\, I_{rh}(t-\tau)\right) + \\ + \left(\frac{1-h}{2}\right)\left(\frac{1+h}{Z}\, e_r(t-\tau) - h\, I_{sh}(t-\tau)\right) \tag{8a}$$

$$I_{rh}(t) = \left(\frac{1+h}{2}\right)\left(\frac{1+h}{Z}\, e_r(t-\tau) - h\, I_{sh}(t-\tau)\right) + \\ + \left(\frac{1-h}{2}\right)\left(\frac{1+h}{Z}\, e_s(t-\tau) - h\, I_{rh}(t-\tau)\right) \tag{8b}$$

where:

$$Z = Z_c + \frac{R}{4}$$

$$h = \frac{Z_c - \frac{R}{4}}{Z_c + \frac{R}{4}}$$

$$Z_c = \sqrt{\frac{L'}{C'}}$$

$$\nu = \frac{1}{\sqrt{L'\,C'}}$$

$$\tau = d\sqrt{L'\,C'}$$

For a lossless line, $R = 0$, $h = 1$, and $Z = Zc$.

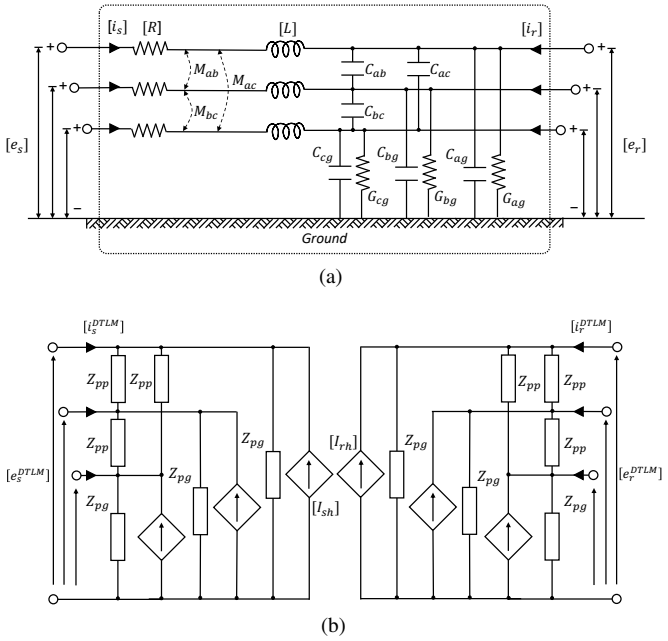

Fig. 2. Three-phase line (a) and the equivalent impedance circuit (b)

B. Three-phase Line

Considering a lossless three-phase line as shown in Figure 2a, Equation 1a and Equation 1b are valid if the scalars are replaced with vectors $[e]$ and $[i]$, and matrices $[L']$ and $[C']$. One of the vector variables can be eliminated by differentiating a second time, which gives Equation 9a and Equation 9b.

$$\left[\frac{\partial^2 e(x,t)}{\partial x^2}\right] = [L']\,[C']\left[\frac{\partial^2 e(x,t)}{\partial t^2}\right] \tag{9a}$$

$$\left[\frac{\partial^2 i(x,t)}{\partial x^2}\right] = [C']\,[L']\left[\frac{\partial^2 i(x,t)}{\partial t^2}\right] \tag{9b}$$

Due to the off-diagonal elements of matrices $[L']$ and $[C']$ that represent the mutual coupling among phases, the solution of Equation 9a and Equation 9b are complicated. To overcome this complexity, a modal transformation could be applied to eliminate mutual dependencies among phases and obtain $[L']$ and $[C']$ in diagonal form. This transformation determines an independent differential equation for each mode that can be solved with the single-phase line algorithm using its modal travel time and its modal surge impedance. Normally, the matrices that apply the transformation are different for voltages and currents as depicted in Equation 10a and Equation 10b.

$$[e_{phase}] = [T_e]\,[e_{mode}] \tag{10a}$$

$$[i_{phase}] = [T_i]\,[i_{mode}] \tag{10b}$$

where $[T_e]$ is the transformation matrix for voltages, and $[T_i]$ for currents. In symmetric three-phase lines, diagonal elements of the matrices $[L']$ and $[C']$ are equal to L'_{self} and C'_{self} and off-diagonals elements are equal to L'_{mutual} and C'_{mutual}. In this cases, a simple transformation is possible, where:

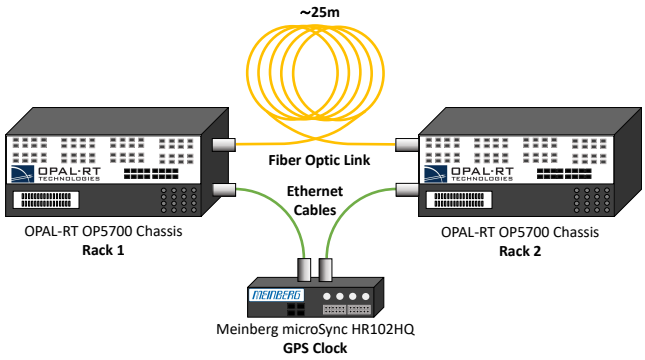

Fig. 3. The locally distributed digital real-time power system co-simulation infrastructure

$$[T_e] = [T_i] = [T] \tag{11}$$

Among the modal transformation described in [22], the power invariant Clarke transformation has been used in our case, obtaining the $\alpha\beta 0$ modes by applying matrix $[T]$ defined in Equation 12 in Equation 10a and Equation 10b.

$$[T] = \sqrt{\frac{2}{3}} \begin{bmatrix} 1 & -\frac{1}{2} & -\frac{1}{2} \\ 0 & \frac{\sqrt{3}}{2} & -\frac{\sqrt{3}}{2} \\ \frac{1}{\sqrt{2}} & \frac{1}{\sqrt{2}} & \frac{1}{\sqrt{2}} \end{bmatrix} \tag{12}$$

The current i_s and i_r entering the left and right line nodes can be written as linear Equations 13a and 13b.

$$[i_s(t)] = [G]\,[e_s(t)] - [I_{sh}(t)] \tag{13a}$$
$$[i_r(t)] = [G]\,[e_r(t)] - [I_{rh}(t)] \tag{13b}$$

These linear equations derive from Equation 5a and Equation 5b by replacing the scalar values i, e, and I with vector $[i]$, $[e]$, and $[I]$ and, finally, substituting $1/Z$ with $[G]$. The final equivalent model is shown in Figure 2b, where Zpg and Zpp are respectively calculated from the equation resulting from nodal analysis of the equivalent model compared to the diagonal and off-diagonals elements of the matrix $[G]$.

III. Methodology

The locally distributed digital real-time power system co-simulation is accomplished by interconnecting two locally distributed DRTS via a bidirectional fiber optic link exploiting Aurora 8B/10B. Aurora is an optical fiber serial link protocol capable of reducing the communication latency among involved DRTS at around hundreds of nanoseconds, ensuring the minimum impact on the co-simulation application. Figure 3 represents the interconnection implemented among two OPAL-RT OP5700 racks. Although the communication latency experienced by the fiber optic link is negligible w.r.t. the DRTS time step duration T_S, the data exchange management among the Aurora channel and the available power system solution cores in DRTS architectures strongly impacts with a latency proportional to T_S depending on the commercial DRTS solution implemented in the co-simulation framework [13].

The time synchronization among the two locally distributed DRTS is ensured by the IEEE 1588 PTP [19]. The IEEE PTP aligns internal clocks of the two DRTS leveraging on a GPS clock. The GPS clock acts as a master of the PTP network sending in broadcast the reference clock received by the GPS signal via different Ethernet ports, each one implementing a different PTP stack configuration. The DRTS must be equipped with a PTP slave board capable of *i)* receiving the synchronization messages coming from the GPS clock, *ii)* calculating the offset, and *iii)* aligning the internal clock of the DRTS. Following the implementation proposed in Figure 3, the infrastructure exploits a Meinberg microSync HR102HQ GPS clock that is interconnected with the two OPAL-RT OP5700 racks by using two Ethernet ports with the same PTP stack configuration. Both OPAL-RT OP5700 racks instead are equipped with an Oregano Syn1588 PTP slave card, offering a single Ethernet port interconnected via an Ethernet cable to one of the two available ports of the Meinberg GPS clock. By laying both on this strategy and on the time synchronization ensured by IEEE PTP stack, the infrastructure exploits the time regulation provided by the real-time constraint of both DRTS without a particular distributed regulation schema.

To cope with the variable latency introduced by the Aurora channel, the PSUT is split by means of a Distributed Transmission Line Model (DTLM) based on Bergeron's travelling wave method [23] used by EMTP [21] and introduced in Section II. By implementing this model, the overall co-simulation latency experienced by the interface signals (i.e. voltages and currents) can be absorbed into the propagation time of the travelling wave, resulting in an identical solution with respect to a monolithic simulation. It is worth noting that the proposed DTLM has intrinsically a limitation of the minimum length of a single-phase line d caused by: *i)* the propagation velocity ν of single-phase line that is related to the characteristic inductance L' and capacitance C' per unit length, and *ii)* the latency τ_{min} experienced from the Aurora communication, normally multiple of the time step duration T_S.

$$d \gg \nu\, \tau_{min} \tag{14}$$

where $\tau_{min} = T_S$ for our locally distributed digital real-time power system co-simulation infrastructure exploiting the OPAL-RT OP5700 racks [13]. The limitation of the minimum length of a three-phase line d instead is related to the highest propagation velocity among the $\alpha\beta 0$ modes resulting from the power invariant Clark transformation [22]. So, Equation 14 becomes:

$$\max_{i \in [\alpha,\beta,0]} d \gg \nu_i\, \tau_{min} \tag{15}$$

A. DTLM Application

This section describes the proposed DTLM block and its generic application in a power system scenario. To achieve the locally distributed digital real-time power system co-simulation, the PSUT must be analysed and a transmission line

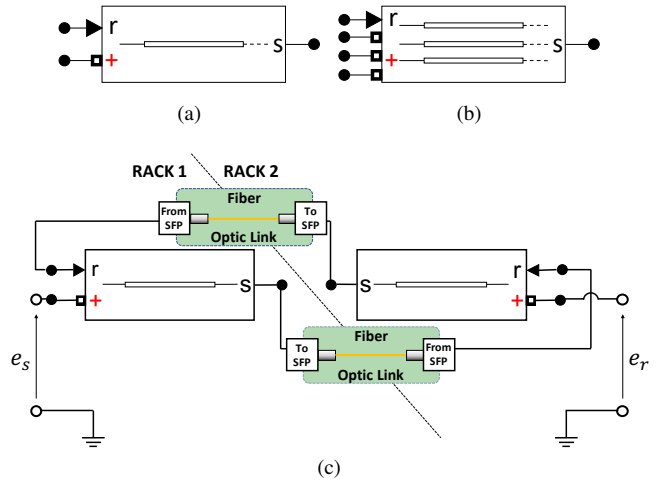

Fig. 4. The DTLM block developed in RT-LAB environment for a single-phase line (a), a three-phase line (b), and its application to decouple a single-phase transmission line (c)

where to split the power system must be identified considering the constraint in Equation 14 for a single-phase line or Equation 15 for a three-phase line. Once selected, the transmission line must be substituted by two DTLM blocks. The DTLM block shown in Figure 4a implements Equations 8b and 8a for the single-phase line in the RT-LAB environment [24], a specific simulation tool to perform modelling of real-time power system for OPAL-RT targets. Figure 4b instead shows the DTLM block for the three-phase line implementing the modal transformation, calculating Equations 8b and 8a for each resulting mode, and anti-transforming to obtain the resulting voltages and currents.

Both blocks present two inputs, namely the voltage input + and the receiving input **r**, and an output **s**, so-called the sending output. The voltage input + receives the electric connection with the power system. The receiving input **r** and the output **s** instead exchange signals with the other block via the Aurora channel to fulfil Equations 8b and 8a and reproduce the transmission line behavior. The single-phase block allows setting different parameters, respectively: *i)* the line length d (km), *ii)* the resistance per unit length R' ($\Omega\,\mathrm{km}^{-1}$), *iii)* the capacitance per unit length C' ($\mathrm{F\,km}^{-1}$), *iv)* the inductance per unit length L' ($\mathrm{H\,km}^{-1}$), *v)* the frequency used for resistive, inductive, and capacitive (RLC) specification f_s (Hz), and *vi)* the communication latency in multiple N of the time step duration T_S. The three-phase block offers similar parameters but requires positive- and zero-sequence values of the resistance, capacitance, and inductance per unit length, respectively $[R'_1, R'_0]$, $[C'_1, C'_0]$, and $[L'_1, L'_0]$.

The communication between the two DTLM blocks for a single-phase line is shown in Figure 4c. The DTLM block of Rack 1 is connected to the left line terminal e_s through the + connector and executes different operations in the same time step, respectively: *i)* it measures the voltage at the left line terminal e_s; *ii)* it receives the output **s** of the DTLM block of Rack 2 via the **r** connector; *iii)* it computes the current i_s imposed to the + connector by solving Equation 8a and Equation 5a; *iv)* it computes the component of Equation 8b excluding e_r voltage contribution; and, finally, *v)* it sends the calculated component from the output connector **s** to let the DTLM block of Rack 2 executing operations *iii)* and *iv)* in the next time steps. The DTLM block of Rack 2 executes the same operations, taking into account the equations related to the right line terminal e_r. As depicted in Figure 4c, the data exchange between **s** and **r** connectors of Rack 1 and 2 happens through the Aurora channel in both directions. To achieve this data exchange, the **s** signal is taken by the **To SFP** block from the real-time simulation environment of a rack that codes and inserts it in the Aurora data stream of the physical fiber optic link. At the receiver side, the stream is decoded and the data is presented into the real-time simulation environment of the other rack via the **From SFP** block. The signal is then redirected to the **r** connector of the DTLM block.

In the three-phase case, the DTLM block is similarly connected to the left line terminal $[e_s]$ through the three-phase + connectors. The executed operations in the same time step are: *i)* it measures the voltages e_s^A, e_s^B, and e_s^C at the left line terminal $[e_s]$; *ii)* it receives **r** that contains r^α, r^β, and r^0 components received from the DTLM block of Rack 2 via the output **s** connector; *iii)* it computes the Clarke transformation of the voltages $[e_s]$ obtaining the modal voltages e_s^α, e_s^β, and e_s^0; *iv)* it computes the current i_s^α, i_s^β, and i_s^0 for each mode by solving Equation 8a and Equation 5a, threatening phase as a single-phase line; *v)* it computes the components s^α, s^β, and s^0 of **r** by applying Equation 8b and excluding $[e_r]$ voltage contribution; *vi)* it applies the Clarke anti-transformation to the current i_s^α, i_s^β, and i_s^0 to obtain i_s^A, i_s^B, and i_s^C; *vii)* it imposes calculated $[i_s]$ as currents to the + connector; and, finally, *viii)* it sends the calculated components s^α, s^β, and s^0 from the output connector **s** to let the three-phase DTLM block of Rack 2 executing operations *iii)* and *vii)* in the next time steps.

IV. Scenario

In the following sections, the scenarios applied to test and evaluate the locally distributed digital real-time power system co-simulation via multi-phase DTLM are described, respectively *i)* the *Single-phase Power System*, and *ii)* the *Three-phase Power System* scenarios.

A. Single-phase Power System

The proposed methodology for single-phase lines is tested over a very simple but effective power system scenario for the re-energization of a transmission line. The monolithic circuit, depicted in Figure 5a, consists of a single-phase voltage source v_S with a standard European voltage level of 380 kV and a nominal frequency of 50 Hz and a source impedance Z_S of magnitude 1 µΩ. To trigger a transient as a case study, a circuit breaker CB, with breaker resistance R_{on} equal to 0.1 Ω and snubber resistance R_s equal to 1 GΩ, positioned after the single-phase voltage source is opened and re-closed after 66.67 ms. The transmission line is a single-phase line of 97.25 km with resistance R', inductance L', and capacitance C' per unit length, respectively: $0.095\,\Omega\,\mathrm{km}^{-1}$, $3.13\,\mathrm{mH\,km}^{-1}$, and $12.39\,\mathrm{nF\,km}^{-1}$. Finally,

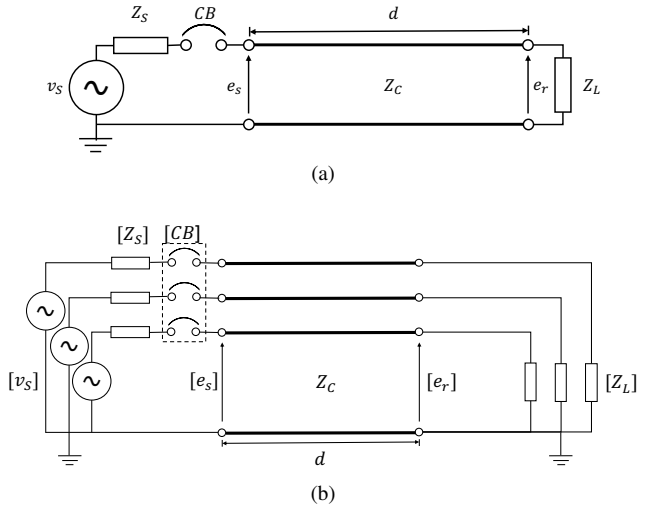

Fig. 5. PSUT composed by a voltage source v_S with pure resistive impedance Z_S, a circuit breaker CB, a single-phase transmission line with characteristic impedance Z_c and length d, and a pure resistive load Z_L (a) and its co-simulated equivalent (b)

the load impedance Z_L is set to $1\,\mathrm{T\Omega}$ to impose an open circuit terminal to the transmission line. The transient that is triggered is therefore the re-energization of a transmission line, in a no-load condition.

The monolithic circuit is split by substituting the transmission line with two DTLM blocks that implement the equivalent impedance network described in Figure 1b. The left and right line terminals, respectively e_s^{DTLM} and e_r^{DTLM}, are represented by two controlled current sources I_{sh} and I_{rh} and their relative surge impedance Z. It is worth noting that the resulting co-simulated equivalent topologically splits the source and load circuit line terminals by indirectly representing the effect of each circuit via the controlled current sources I_{sh} and I_{rh}. This permits to run the circuits on two different DRTS racks and exchanging the component described in Section III-A via the proposed locally distributed digital real-time power system co-simulation to update and calculate the corresponding i_s^{DTLM} and i_r^{DTLM}.

B. Three-phase Power System

The proposed methodology for three-phase lines is tested over the same power system scenario for the single-phase line presented in the previous Section II-A declined into a three-phase system. The three-phase voltage source v_S has a standard European voltage level of $380\,\mathrm{kV}$ and a nominal frequency of $50\,\mathrm{Hz}$ with the same series source impedances Z_S of magnitude $1\,\mu\Omega$ for each phase. To trigger the transient, the three-phase circuit breaker CB, with breaker resistance R_{on} equal to $0.1\,\Omega$ and snubber resistance R_s equal to $1\,\mathrm{G\Omega}$, positioned after the three-phase voltage source is opened and re-closed after $66.67\,\mathrm{ms}$. The transmission line is a three-phase line of $97.25\,\mathrm{km}$ with positive- and zero-sequence resistances $[R'_1, R'_0]$, inductances $[L'_1, L'_0]$, and capacitances $[C'_1, C'_0]$ per unit length, respectively: $[0.01273 \quad 0.3864]\ \Omega\,\mathrm{km}^{-1}$, $[0.9337\ 4.1264]\ \mathrm{mH\,km}^{-1}$, and $[12.74\ 7.751]\ \mathrm{nF\,km}^{-1}$. The load imposes an open circuit terminal to the transmission line with a three-phase series impedance Z_L set to $1\,\mathrm{T\Omega}$.

The circuit is split by substituting the transmission line with two DTLM blocks that implement the equivalent impedance network described in Figure 2b. The left and right line terminals, respectively $[e_s^{DTLM}]$ and $[e_r^{DTLM}]$, are represented by three controlled current sources $[I_{sh}]$ for the left side of the circuit and three controlled sources $[I_{rh}]$ for the right side of the circuit. Moreover, each phase has a relative surge impedance Z_{pg} and a mutual surge impedance Z_{pp}. Their values are automatically calculated during the initialization of the DTLM block. It is worth noting that the resulting three-phase co-simulated equivalent topologically splits the source and load circuit line terminals by indirectly representing the effect of each circuit via the controlled current sources $[I_{sh}]$ and $[I_{rh}]$. This permits to run the circuits on two different DRTS racks and exchanging the component described in Section III-A via the proposed locally distributed digital real-time power system co-simulation to update and calculate the corresponding $[i_s^{DTLM}]$ and $[i_r^{DTLM}]$.

V. Experimental Results

The proposed locally distributed digital real-time power system co-simulation is implemented in a testbed involving two OPAL-RT OP5700 racks, as depicted in Figure 3. This configuration provides a co-simulation infrastructure with an optical fiber optic link of 25 meters between SFP Port 0 of Rack 1 and SFP Port 0 of Rack 2. The time synchronisation, alignment, and regulation schema of the co-simulation infrastructure are offered by the IEEE 1588 PTP stack. Indeed, the testbed exploits a Meinberg microSync HR102HQ GPS Clock as a master clock of the PTP network. The GPS Clock can synchronise the internal clocks of both racks with an offset of tens of nanoseconds, which is enough to consider negligible their misalignment with respect to the time step duration. To receive the PTP messages, the OPAL-RT OP5700 racks must be equipped with an Oregano Syn1588 PCIe NIC card that allows setting the racks as slaves of the PTP networks. The PTP stack is an IEEE 1588-2008 v2 Default Layer 2 profile with End-to-End (E2E) Transparent Clock (TC).

Over the 25-meters fiber optic link, Aurora 8B/10B is enabled in the RT-LAB environment by using the **From SFP** and **To SFP** block, two *OpCtrl* blocks that allow defining: i) the *SFP Port Number* of the front panel of the rack, and ii) the *Data Width* of the channel in numbers of double variables. The power system scenarios presented in Section IV, namely *i)* the Single-phase Power System and *ii)* the Three-phase Power System, are developed in the RT-LAB environment in both the monolithic simulation and locally distributed co-simulation configurations. The monolithic power systems in Figure 5a and Figure 5b have been run simultaneously with the co-simulated cases on Rack 1 in order to compare them with the co-simulation results. The experiment is run at a time step duration T_S of $50\,\mu\mathrm{s}$, a typical EMT analysis setting for sufficient details of the transient. In the following sections, the experimental results of the two scenarios are extensively discussed.

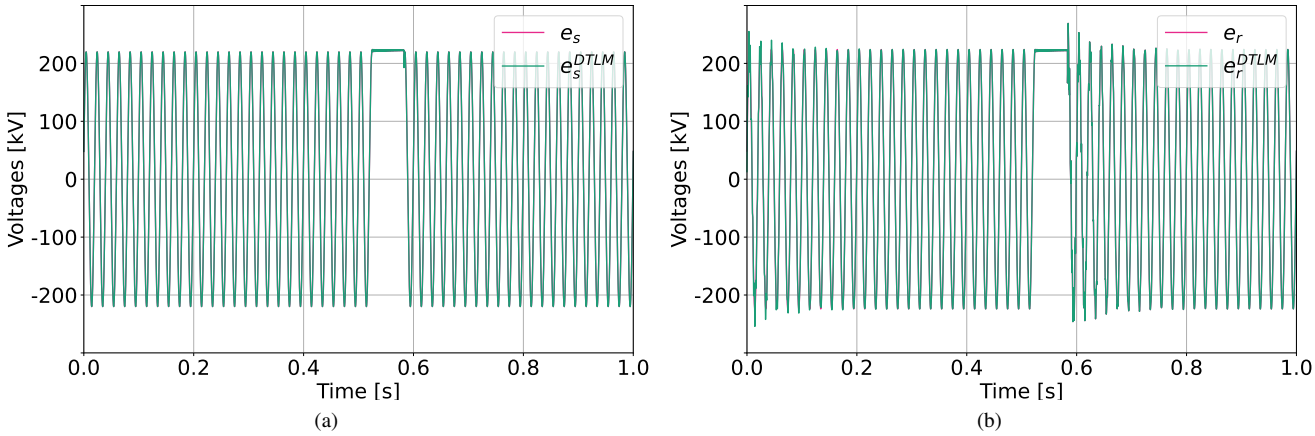

Fig. 6. Voltage plots of the transient generated by the re-energization of the single-phase transmission line for the monolithic and co-simulated scenarios with a time step duration $T_s = 50\,\mu s$ for the left terminal (a) and right terminal (b) of the line

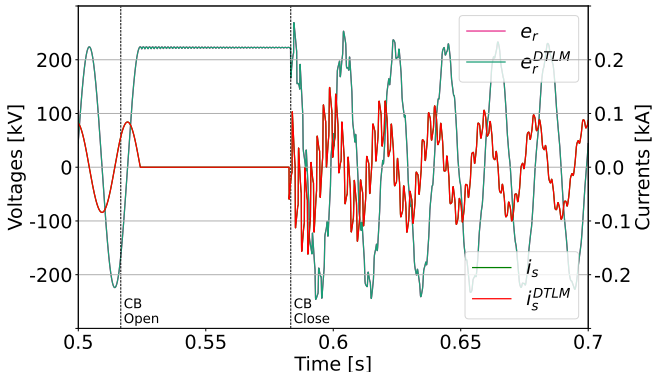

Fig. 7. Right terminal voltages (i.e. e_r and e_r^{DTLM}) and left terminal currents (i.e. i_s and i_s^{DTLM}) transient generated by the re-energization of the single-phase transmission line for the monolithic and co-simulated scenario with a time step duration $T_s = 50\,\mu s$

A. Single-phase Power System

Figure 6 presents the time domain accuracy results among the monolithic and co-simulated power systems. Figure 6a presents the comparison among e_s and e_s^{DTLM}. The voltages e_s^{DTLM} of the co-simulated scenario accurately reproduce the monolithic scenario without significant error w.r.t. e_s. In fact, the Mean Absolute Percentage Error (MAPE) defined in Equation 16 is equal to $0.689\,\%$.

$$MAPE = \frac{100}{N}\sum_{i=1}^{N}\left|\frac{e_i - e_i^{DTLM}}{e_i}\right| \tag{16}$$

where N is the total number of simulation time steps, e_i are the monolithic voltage results, and e_i^{DTLM} are the co-simulated voltage results.

The same result is achieved when comparing e_r and e_r^{DTLM} in Figure 6b, where e_r^{DTLM} reproduce precisely e_r with a MAPE value of almost $0.0026\,\%$. It is worth noting that both e_r and e_r^{DTLM} present an initial transient due to the fact that the monolithic circuit implements a distributed parameter model for the transmission line. This effect refers to the empty memory of the model at the beginning of the experiments. In fact, both the distributed parameter model of the monolithic scenario and the DTLM memories of the co-simulated scenario are initialised to zero. e_r and e_r^{DTLM} show an initial peak with a rise of $113.9260\,\%$ compared to the nominal voltage and the distortion transient lasts almost 5 cycles before disappearing.

Figure 7 shows the transients generated by the re-energization of the transmission line in the no-load condition for left terminal currents (i.e. i_s and i_s^{DTLM}) and the right terminal voltage (i.e. e_r and e_r^{DTLM}), which present the most interesting transients that could depict DTLM issues in reproducing high-frequency details. Once the open command arrives at the circuit breaker CB at $t = 0.516\,67\,s$, the opening of the line takes place at the first zero-crossing condition of the current i_s that is $t = 0.525\,s$ to avoid arc generations. At this point, the current at the sending terminal remains zero until the breaker is re-closed. Vice-versa, the voltage at the receiving terminal remains constant, at $311.126\,kV$, because in the line model, the shunt conductance G is neglected and the shunt capacitance C remains charged. When the CB is closed again, a re-energization transient is triggered, with some oscillations due to the line parameters.

The precision in reproducing the monolithic results is also appreciable in Figure 7, where all DTLM voltage and currents plots overlay the standalone ones with high accuracy.

B. Three-phase Power System

In Figure 8, the time domain accuracy results among the monolithic and co-simulated three-phase power systems are presented. Figures 8a, 8c, and 8e present the comparison among $[e_s]$ and $[e_s^{DTLM}]$ respectively for phase A, B, and C. The voltages e_s^{ADTLM}, e_s^{BDTLM}, and e_s^{CDTLM} of the co-simulated scenario accurately reproduce the monolithic scenario without significant error w.r.t. e_s^A, e_s^B, and e_s^C. In fact, the values of the MAPE defined in Equation 16 are equal to $0.0028\,\%$ for phase A, $0.0019\,\%$ for phase B, and $0.0018\,\%$ for phase C.

The same result is achieved when comparing $[e_r]$ and $[e_r^{DTLM}]$ in Figures 8b, 8d, and 8f where e_r^{ADTLM} reproduce precisely e_r^A with a MAPE value of almost $1.3584\,\%$.

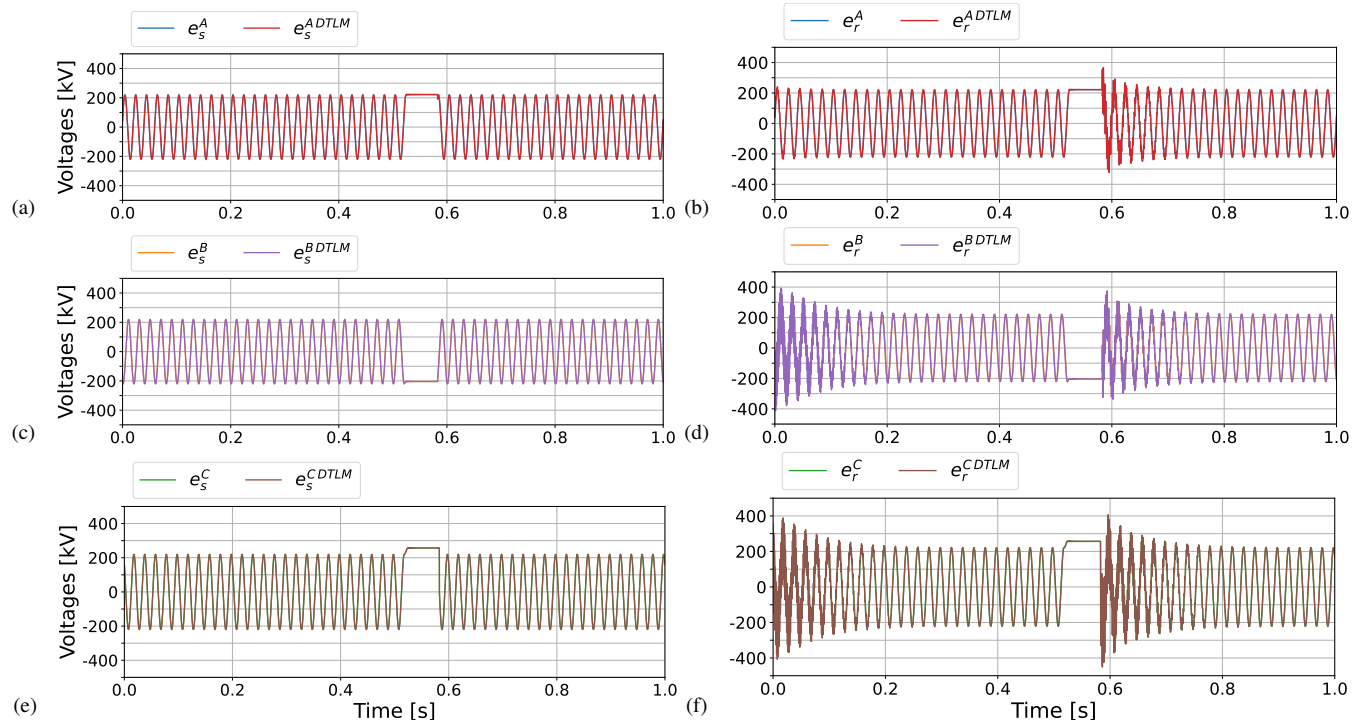

Fig. 8. Voltage plots of the transient generated by the re-energization of the three-phase transmission line for the monolithic and co-simulated scenarios with a time step duration $T_s = 50\,\mu s$ for the left terminal (a) and right terminal (b) of the line

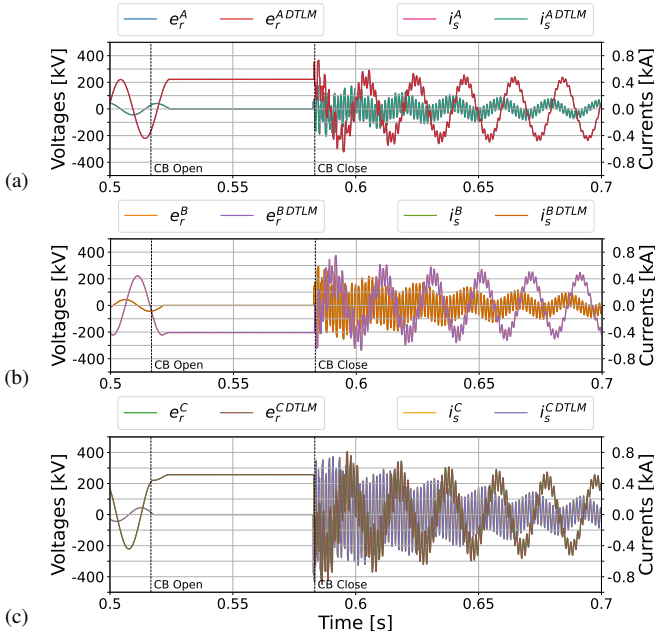

Fig. 9. Right terminal voltages (i.e. e_r and e_r^{DTLM}) and left terminal currents (i.e. i_s and i_s^{DTLM}) transient generated by the re-energization of the three-phase transmission line for the monolithic and co-simulated scenario with a time step duration $T_s = 50\,\mu s$

e_r^{BDTLM} instead reproduce e_r^B with a MAPE value of nearly $4.3192\,\%$. Similarly, e_r^{CDTLM} reproduce e_r^C with a MAPE value of around $4.6151\,\%$. As in the single-phase DTLM, this effect refers to the delay (i.e. memory) involved in reproducing the travelling wave of each phase at the beginning of the experiments. In fact, the distributed parameter model of the monolithic scenario and the DTLM memories of the co-simulated scenarios are initialised to zero. This initialization affects the results with nonlinearities provoking a triangle wave superimposed to the original sinusoid that absorbs after an initial transient.

The initial transient voltage peak for each phase is affected by the different initial phase conditions of $[e_r]$ and $[e_r^{DTLM}]$. For phase A, e_r^A and e_r^{ADTLM} show an initial peak with a rise of $108.7939\,\%$ compared to the nominal voltage and the distortion transient lasts almost 4 cycles before disappearing. e_r^B and e_r^{BDTLM} instead present an initial negative peak with a rise of $186.1832\,\%$ compared to the nominal voltage and the distortion transient lasts around 8 cycles. Finally, e_r^C and e_r^{CDTLM} overpeak is around $183.8545\,\%$ from the nominal voltage and, similarly to phase B, the distortion transient lasts around 8 cycles.

Figure 9 shows the transients generated by the re-energization of the three-phase transmission line in the no-load condition for left terminal currents (i.e. $[i_s]$ and $[i_s^{DTLM}]$) and the right terminal voltage (i.e. $[e_r]$ and $[e_r^{DTLM}]$), which present the most interesting transients that could depict DTLM issues in reproducing high-frequency details. Once the open command arrives at the circuit breaker CB at $t = 0.516\,67\,\mathrm{s}$, the opening of the lines takes place at the first zero-crossing condition of the current $[i_s]$ to avoid arc generations, that are $t = 0.524\,\mathrm{s}$ for phase A, $t = 0.521\,\mathrm{s}$ for phase B, and $t = 0.5175\,\mathrm{s}$ for phase C. At this point, the current measured at the sending terminal remains zero until the breaker is re-closed. Vice-versa, the voltage measured at the receiving terminal remains constant, at $311.126\,\mathrm{kV}$, because in the line model, the shunt conductance G is neglected and the shunt

capacitance C remains charged. When the CB is closed again, a re-energization transient is triggered, with damped oscillations due to the line parameters.

The precision in reproducing the three-phase monolithic results is also appreciable in Figure 9, where all DTLM voltage and currents plots overlay the standalone ones with high accuracy.

VI. Conclusion

A locally distributed digital real-time power system co-simulation via the application of a Multi-phase Distributed Transmission Line Model (DTLM) was presented. The application of the DTLM ensures stability and accuracy of the numerical solution of a PSUT with results identical to a monolithic real-time simulation with the constraints of Equation 14 for the single-phase case and Equation 15 for the three-phase case. The proposed infrastructure that adopts the Aurora protocol for communication guarantees the minimum latency and the lowest constraints of the minimum distance of the transmission line to be substituted by the DTLM. The IEEE 1588 PTP instead ensures the proper alignment, synchronization, and regulation of the internal clock of the locally distributed DRTS, thus allowing the proper alignment of the experimental result too. Two simple but effective scenarios with a simulation time step of $50\,\mu s$ has been analysed to assess the time-domain accuracy of the solution, respectively one for the single-phase DTLM block and one for the three-phase DTLM block. The multi-phase DTLM replicates precisely and with the highest accuracy in reproducing the behaviour of the monolithic power system for both scenarios. The interconnection was tested on two DRTS (i.e. OPAL-RT OP5700) with a 25-meter fiber optic link. Future works will involve interconnecting different types of DRTS with the proper time synchronization, alignment, and regulation capability of the IEEE 1588 PTP protocol in order to expand the computational capabilities of individual laboratories. Moreover, the proposed infrastructure only permits the interconnection of locally distributed DRTS. In future works, geographically distributed interconnection with different laboratories will be integrated with the locally distributed capability of our infrastructure. Finally, a more complex scenario will be investigated involving synchronous generators on both sides of the PSUT to test the alignment of the start-up of the experiments on both DRTS.

Acknowledgments

This work was partially supported by the EU H2020 Project *European Research Infrastructure supporting Smart Grid and Smart Energy Systems Research, Technology Development, Validation and Roll Out - Second Edition (EriGRID2.0)*, Grant Agreement N^o 654113.

References

[1] European Commission, "Communication from the Commission to the European Parliament, the Council, the European Economic and Social Committee and the Committee of the Regions Powering a Climate-Neutral Economy: An Eu Strategy for Energy System Integration." [Online]. Available: https://eur-lex.europa.eu/legal-content/EN/ALL/?uri=COM:2020:299:FIN

[2] B. Ahmed, A. Abdelgadir, N. A. Saied, and A. A. Karrar, "A Compensated Distributed-Parameter Line Decoupling Approach for Real-Time Applications," *IEEE Transactions on Smart Grid*, vol. 12, no. 2, pp. 1761–1771, 2021.

[3] The MathWorks, Inc. Simscape Electrical. [Online]. Available: https://it.mathworks.com/help/sps/index.html

[4] C. Dufour and G. Sapienza, "Testing 750 node distribution grids and devices," in *2015 International Symposium on Smart Electric Distribution Systems and Technologies (EDST)*, 2015, pp. 572–578.

[5] OPAL-RT Technologies, Inc. Advanced Real-Time ElectroMechanical Simulator (ARTEMiS). [Online]. Available: https://wiki.opal-rt.com/display/Artemis/

[6] M. D. Omar Faruque, T. Strasser, G. Lauss, V. Jalili-Marandi, P. Forsyth, C. Dufour, V. Dinavahi, A. Monti, P. Kotsampopoulos, J. A. Martinez, K. Strunz, M. Saeedifard, X. Wang, D. Shearer, and M. Paolone, "Real-Time Simulation Technologies for Power Systems Design, Testing, and Analysis," *IEEE Power and Energy Technology Systems Journal*, vol. 2, no. 2, pp. 63–73, 2015.

[7] A. van der Meer, P. Palensky, K. Heussen, D. Morales Bondy, O. Gehrke, C. Steinbrinki, M. Blanki, S. Lehnhoff, E. Widl, C. Moyo, T. Strasser, V. Nguyen, N. Akroud, M. Syed, A. Emhemed, S. Rohjans, R. Brandl, and A. Khavari, "Cyber-physical energy systems modeling, test specification, and co-simulation based testing," in *2017 Workshop on Modeling and Simulation of Cyber-Physical Energy Systems (MSCPES)*, 2017, pp. 1–9.

[8] M. H. Syed, E. Guillo-Sansano, Y. Wang, S. Vogel, P. Palensky, G. M. Burt, Y. Xu, A. Monti, and R. Hovsapian, "Real-Time Coupling of Geographically Distributed Research Infrastructures: Taxonomy, Overview, and Real-World Smart Grid Applications," *IEEE Transactions on Smart Grid*, vol. 12, no. 2, pp. 1747–1760, 2021.

[9] J. Montoya, R. Brandl, K. Vishwanath, J. Johnson, R. Darbali-Zamora, A. Summers, J. Hashimoto, H. Kikusato, T. S. Ustun, N. Ninad, E. Apablaza-Arancibia, J.-P. Bérard, M. Rivard, S. Q. Ali, A. Obushevs, K. Heussen, R. Stanev, E. Guillo-Sansano, M. H. Syed, G. Burt, C. Cho, H.-J. Yoo, C. P. Awasthi, K. Wadhwa, and R. Bründlinger, "Advanced Laboratory Testing Methods Using Real-Time Simulation and Hardware-in-the-Loop Techniques: A Survey of Smart Grid International Research Facility Network Activities," *Energies*, vol. 13, no. 12, 2020. [Online]. Available: https://www.mdpi.com/1996-1073/13/12/3267

[10] M. Syed, T. T. Hoang, A. C. Kontou, A. G. Paspatis, G. M. Burt, Q. T. Tran, E. Guillo-Sansano, S. Vogel, H. T. Nguyen, and N. D. Hatziargyriou, "Applicability of Geographically Distributed Simulations," *IEEE Transactions on Power Systems*, vol. 38, no. 4, pp. 3107–3122, 2023.

[11] E. Buraimoh, G. Ozkan, L. Timilsina, P. K. Chamarthi, B. Papari, and C. S. Edrington, "Overview of Interface Algorithms, Interface Signals, Communication and Delay in Real-Time Co-Simulation of Distributed Power Systems," *IEEE Access*, vol. 11, pp. 103 925–103 955, 2023.

[12] Z. Feng, R. Peña-Alzola, P. Seisopoulos, E. Guillo-Sansano, M. Syed, P. Norman, and G. Burt, "A Scheme to Improve the Stability and Accuracy of Power Hardware-in-the-Loop Simulation," in *IECON 2020 The 46th Annual Conference of the IEEE Industrial Electronics Society*, 2020, pp. 5027–5032.

[13] L. Barbierato, E. Pons, E. F. Bompard, V. S. Rajkumar, P. Palensky, L. Bottaccioli, and E. Patti, "Exploring Stability and Accuracy Limits of Distributed Real-Time Power System Simulations via System-of-Systems Cosimulation," *IEEE Systems Journal*, pp. 1–12, 2023.

[14] Z. Shen, F. Arraño-Vargas, H. R. Wickramasinghe, and G. Konstantinou, "Development of Power System Models for Distributed Real-Time Simulations," *IEEE Access*, vol. 10, pp. 119 706–119 721, 2022.

[15] A. Aguirre, M. Davila, P. Zuniga, F. Uribe, and E. Barocio, "Improvement of damping impedance method for Power Hardware in the Loop simulations," in *2016 IEEE International Autumn Meeting on Power, Electronics and Computing (ROPEC)*, 2016, pp. 1–6.

[16] M. Stevic, A. Estebsari, S. Vogel, E. Pons, E. Bompard, M. Masera, and A. Monti, "Multi-Site European framework for real-time co-simulation of power systems," *IET GENERATION TRANSMISSION and DISTRIBUTION*, vol. 11, no. 17, pp. 4126–4135, 2017.

[17] M. Stevic and A. Monti, "Wave Transformation Based Interface Algorithm for Distributed Simulation of HVDC Systems," in *IECON 2018 - 44th Annual Conference of the IEEE Industrial Electronics Society*, 2018, pp. 4019–4023.

[18] E. Guillo-Sansano, M. H. Syed, A. J. Roscoe, G. M. Burt, and F. Coffele, "Characterization of Time Delay in Power Hardware in the Loop Setups," *IEEE Transactions on Industrial Electronics*, vol. 68, no. 3, pp. 2703–2713, 2021.

[19] "IEEE Standard for a Precision Clock Synchronization Protocol for Networked Measurement and Control Systems," *IEEE Std 1588-2008 (Revision of IEEE Std 1588-2002) - Redline*, pp. 1–300, 2008.
[20] L. Barbierato, S. Vogel, D. S. Schiera, E. Pons, L. Bottaccioli, A. Monti, and E. Patti, "Digital Real-Time Power System Co-simulation via Distributed Transmission Line Model," in *2023 IEEE International Conference on Environment and Electrical Engineering and 2023 IEEE Industrial and Commercial Power Systems Europe (EEEIC / ICPS Europe)*, 2023, pp. 1–6.
[21] H. W. Dommel, "Digital Computer Solution of Electromagnetic Transients in Single-and Multiphase Networks," *IEEE Transactions on Power Apparatus and Systems*, vol. 88, pp. 388–399, 1969.
[22] C. J. O'Rourke, M. M. Qasim, M. R. Overlin, and J. L. Kirtley, "A Geometric Interpretation of Reference Frames and Transformations: dq0, Clarke, and Park," *IEEE Transactions on Energy Conversion*, vol. 34, no. 4, pp. 2070–2083, 2019.
[23] *Du coup de bélier en hydraulique au coup de foudre en électricité: méthode graphique générale, author=Bergeron, L.J.B.* Dunod, 1949.
[24] OPAL-RT Technologies, Inc. RT-LAB. [Online]. Available: https://www.opal-rt.com/software-rt-lab/